MDPI

Article

A Robust Vector-Tracking Loop Based on KF and RTS Smoothing for Shipborne Navigation

Yuan Hu [1], Linjin Wu [1], Naiyuan Lou [2] and Wei Liu [2,*]

1 College of Engineering Science and Technology, Shanghai Ocean University, Shanghai 201306, China; y-hu@shou.edu.cn (Y.H.); m210811433@st.shou.edu.cn (L.W.)
2 Merchant Marine College, Shanghai Maritime University, Shanghai 201306, China; 202240110003@stu.shmtu.edu.com
* Correspondence: liu.wei@shmtu.edu.cn

Abstract: High-precision navigation systems are crucial for unmanned autonomous vessels. However, commonly used Global Navigation Satellite System (GNSS) signals are often severely affected by environmental obstruction, leading to reduced positioning accuracy or even the inability to locate. To address the issues caused by signal obstruction in high-precision navigation systems, the research presented in this paper proposes a vector-tracking loop (VTL) structure based on the forward Kalman Filter (KF) and the backward Rauch Tung Striebel (RTS) smoothing algorithm. The introduction of loop filters in the signal-tracking loop improves the tracking accuracy of the carrier and code, thereby enhancing the stability and robustness of the navigation system. The traditional scalar-tracking loop (STL), traditional VTL, and Kalman Filter (KF)-based VTL were compared through shipborne motion experiments, and the proposed method demonstrated superior signal-tracking capability and navigation accuracy. In the experiment, there were three blocking areas along the experimental path. The experimental results show that, when there are signal blockages of 12 s, 18 s, and 40 s, compared to the traditional VTL method, the proposed method can reduce the horizontal position error by 93.9%, 95.8%, and 94.5%, respectively, as well as the horizontal velocity error by 71.1%, 95.8%, and 97.6%, respectively.

1. Introduction

The emergence of unmanned ships represents a significant transformation in the maritime transportation industry, heralding an important development path for future maritime traffic. The core of this technology lies in achieving comprehensive unmanned management of maritime operations through advanced remote-control systems and intelligent autonomous decision-making capabilities of the ships themselves. With continuous technological advancements, unmanned ships are expected to play a significant role in ocean transportation, maritime search and rescue, and environmental monitoring. To achieve precise control of unmanned vessels and real-time decision-making assistance for vessel movement, a high-precision ship navigation system is essential. The Global Navigation Satellite System (GNSS) provides real-time navigation information to global users through radio waves and is currently the most widely utilized system in the field of maritime navigation. Although the application of GNSS as a navigation system in the maritime field is very common, some issues still need to be addressed for maritime use. Currently, unmanned vessels mainly operate in relatively complex environments, such as nearshore or inland waterways, which is different from ocean-going ships that operate in open seas. In these scenarios, GNSS signals are often affected by external interference, such as buildings, bridges, trees, and complex electromagnetic environments, leading to a significant decrease in the positioning accuracy of the navigation systems.

Scholars have also conducted technical research to address the impact of signal obstruction on navigation systems. Some scholars have focused on improving the anti-interference capability of receivers by optimizing signal-processing algorithms and enhancing the receiver hardware performance to reduce noise problems in weak-signal environments, thereby improving the stability and positioning accuracy of navigation systems. Other scholars have focused on using auxiliary data sources, such as ground station networks or satellite augmentation systems, to enhance the robustness and reliability of navigation systems in complex environments. In addition, some scholars are researching the use of other navigation sensor data sources to achieve multisource integrated navigation systems. In conclusion, various technical studies in different directions are actively underway to address the impact of signal obstructions on navigation systems.

The research presented in this paper proposes a vector-tracking loop (VTL) algorithm structure based on forward Kalman Filter (KF) and the backward Rauch Tung Striebel (RTS) smoothing algorithm to enhance the tracking capability of shipborne navigation receivers in weak-signal environments and improve the robustness and navigation accuracy of shipborne navigation systems. The innovations of this paper are summarized as follows:

A tracking loop filter was designed based on a combination of Kalman Filter (KF) forward filtering and backward RTS smoothing algorithms, aiming to improve the tracking accuracy of the carrier and code in VTL. Stable signal tracking in obstructed environments was achieved by improving the tracking accuracy of the loop, thus enhancing navigation accuracy. To evaluate the performance of the proposed VTL, motion experiments on board ships were designed, and the navigation performances of traditional scalar-tracking loops (STLs), traditional VTL, and KF-based VTL were evaluated. The results of the experiment indicate that the proposed method demonstrates a superior performance compared with the other three methods in terms of signal tracking, accuracy of navigation position, and velocity.

2. Related Works

Traditional GNSS receivers use scalar-tracking loops to process satellite signals. A scalar-tracking loop is a simple feedback control system that is used to separately track the pseudocode phase error and carrier frequency error of each satellite signal. In this tracking mode, the processing of each satellite signal is independent, and there is no information exchange or fusion [1]. STL focuses only on the strength changes in individual satellite signals and maintains synchronization with the satellite signal by adjusting the frequency and phase of the local oscillator. This single-channel tracking method makes handling multiple satellite signals relatively easy. However, the drawback of STL is that it cannot analyze the signal quality deeply. It cannot distinguish between directly received satellite signals and multipath signals caused by reflections from the surrounding environment; therefore, its tracking accuracy is affected in cases of severe multipath effects or signal obstruction. Additionally, STL cannot utilize information from different channels for cross-validation or assistance, thus limiting its performance in complex environments. Researchers have proposed a new vector-tracking loop (VTL) structure to solve the signal-tracking problem in complex environments. This structure utilizes advanced technology and algorithms to accurately track signals in complex and changing environments, and it exhibits strong anti-interference capabilities [2,3]. VTL controls the joints of all tracked satellite signal channels through navigation fusion filters, thus fully utilizing the common information between each channel [4]. This feature enables the VTL to better track weak signals and highly dynamic signals without adding external hardware assistance, and it also exhibits a higher tracking performance under multipath and non-line-of-sight signal conditions [5]. Therefore, VTL is a solution to unstable signal tracking in weak-signal scenarios and has important research significance. Some scholars have made improvements to the signal-tracking loop of VTL and introduced new filtering schemes and optimized algorithms to improve the tracking accuracy of the loop for carriers and code. To reduce the impact of weak signals on the vector-tracking loop and improve navigation accuracy,

Kim et al. proposed a new tracking-loop structure. They used local filtering linear filters and covariance scaling methods to mitigate the influence of weak signals on the entire system, resulting in a good signal-tracking performance [6]. To improve the stability of the vector-tracking loop, Lin et al. proposed a loop tracking structure based on a diagonal weighting matrix. The simulation shows that even though the accuracy of the navigation results is slightly lost, the system can obtain strong robustness [7]. Reducing the frequency error of signal tracking is also a way to improve system stability. Park et al. designed the loop structure of the LQG-VTL and calculated the total frequency tracking error to determine the control gain matrix in the algorithm structure. Finally, by comparing the EKF-VTL method with the simulation, the LQG-VTL method was found to have better system robustness [8]. Liu et al. proposed a vector-tracking framework based on FLS-VTL to solve the problem of the signal loop losing lock under signal occlusion by using the intermediate pseudo-range error and pseudo-range rate error in the calculation process of the software receiver as the input parameters of the navigation processor to solve the navigation results. This method improved the signal-tracking capability of the system. It also improved the navigation precision to a certain extent [9]. Xia et al. proposed a vector-tracking algorithm based on VDFLL, which has a good effect on preventing signal fluctuations caused by ionospheric scintillation, making the signal-tracking loop perform well even in the case of strong ionospheric scintillation [10]. These methods not only enhance the noise-suppression capability of the signal processing system but also strengthen the anti-interference ability of the system. In addition, they have adopted advanced digital signal-processing techniques to effectively reduce multipath interference in the signal and have demonstrated good stability and reliability in complex electromagnetic environments. These technological innovations provide reliable, stable, and efficient solutions for the practical application of VTL. However, current research on the performance of VTL methods mainly focuses on improving the anti-interference ability, stability, and robustness of the system and does not comprehensively evaluate the accuracy of the entire navigation system from signal capture and tracking and navigation results. At the same time, few studies have conducted actual motion experiments to evaluate the performance of the proposed method.

The navigation processor is generally used to process the data signal after loop filtering and to calculate the user's position, velocity, and time [9]. Its main tasks include decoding and parsing the pseudo range, Doppler frequency shift, and orbit information in satellite signals, as well as performing various algorithms to estimate the three-dimensional position of the receiver [11]. In addition, to improve positioning accuracy and robustness, the navigation processor must also filter the signal data, correct errors, and perform fault detection and fault-tolerant processing. Many scholars have improved the working principle of navigation processors by optimizing their internal filtering algorithms to achieve high-precision navigation. Dai et al. proposed an adaptive navigation processor to suppress signal interference in harsh environments [12]. Jakubov et al. introduced a federal filtering method in their study in which the main filter was used as a navigation processor to feed back the navigation parameters of the receiver. The experimental results show that the performance of the federal filter loop is better than that of the KF loop, which reduced computational complexity and improved the robustness of the system [13].

The integration navigation technology based on multiple sensors is currently an effective way to achieve high-precision navigation [14]. In addition to incorporating the Inertial Navigation System (INS) and Celestial Navigation System (CNS), it can also integrate various types of sensor information, such as map data and radar, to enhance the stability and reliability of the navigation system. Gan et al. deduced a mathematical model of GNSS/INS-integrated navigation in their research and summarized the navigation state and measurement model in the algorithm [15]. Liu et al. proposed an ultra-tightly coupled integration system architecture based on INS and GNSS that can effectively suppress error divergence and signal lock-out [16]. Qin et al. proposed a low-cost VTL/IMU-integrated navigation structure based on the principle of integrated navigation, which has a good dynamic performance [17]. Furthermore, utilizing advanced algorithms and models to

fuse different sensor data can effectively mitigate the errors and drift issues present in individual sensors, thereby meeting the high-precision navigation requirements across various application scenarios. Zhu et al. explored the tight integration scheme of GNSS/INS in their research, designed a set of low-cost GNSS/INS-integrated navigation systems using multiple receivers, reduced the calculation amount of the system through a differential calculation method, and conducted experiments and performance evaluations [18]. This multisource fusion combination navigation technology holds promising prospects for wide applications in fields such as unmanned driving [19], aerospace, and ocean exploration. However, the integrated navigation system still has shortcomings and research bottlenecks. The use of multiple systems increases the computational pressure on navigation processors. The accuracy of the IMU also significantly limits the navigation accuracy of the combined system. At the same time, a deeply integrated navigation system is still in the research stage and cannot be applied. Therefore, the proposed robust vector-tracking method can effectively improve navigation accuracy and system stability without increasing the computational burden of the processor, which is worthy of extensive research and attention.

3. GNSS Signal-Tracking Loop

To achieve high-precision navigation and positioning of GNSS in occluding environments and overcome weak satellite signals, multipath effects, and non-line-of-sight environment interference, a new VTL structure is proposed. The structure combines forward KF filtering and reverse RTS fixed-interval smoothing algorithms. The structural principle of the proposed algorithm is illustrated in Figure 1. The main research content of this paper is indicated in the figure with a red box.
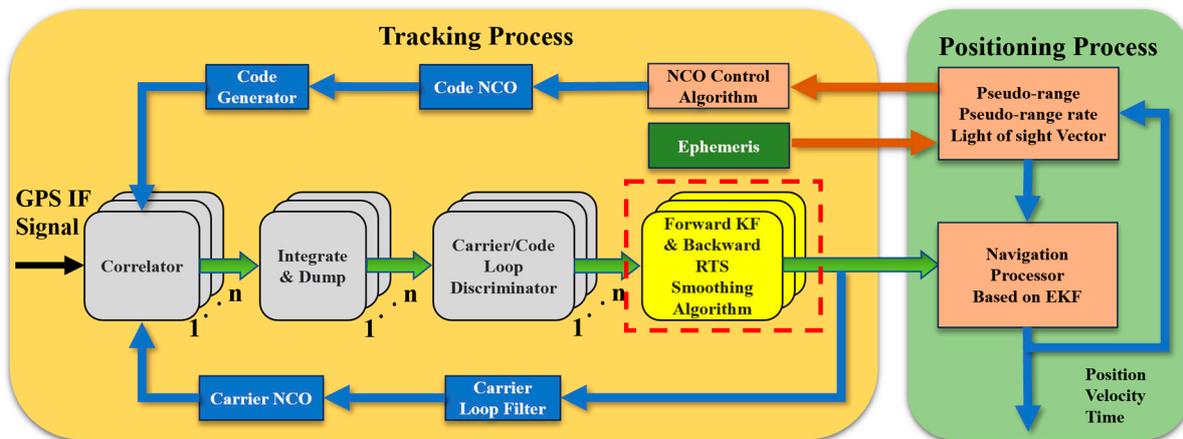

Figure 1. Proposed KF and RTS VTL architecture.

3.1. Signal-Tracking Loop Based on Forward KF

Studies have shown that the Kalman Filter is used to accurately estimate the system state of the receiver in the vector-tracking loop and to predict possible errors, thus significantly enhancing the tracking performance of the tracking loop [20]. This method significantly improves the accuracy of navigation and positioning, particularly in environments where the satellite signal strength is weak. In the Kalman Filter algorithm of the vector-tracking loop, the observation equation, X, for the following loop state variables is constructed, where $\Delta\tau$ (chips) represents the code phase error, $\Delta\phi$ (rad) represents the carrier phase error, Δf (Hz) represents the carrier frequency error, and $\Delta\dot{f}$ (Hz/s) represents the carrier frequency rate error. The discrete system state model is as follows [2,21]:

$$X_k^i = \Phi_{k/k-1} X_{k-1}^i + W_k^i \tag{1}$$

$$X^i = [\Delta\tau^i, \Delta\phi^i, \Delta f^i, \Delta\dot{f}^i] \tag{2}$$

$$\Phi_{k/k-1} = \begin{bmatrix} 1 & 0 & \beta T & \beta\frac{T}{2} \\ 0 & 1 & 2\pi T & \pi T^2 \\ 0 & 0 & 1 & T \\ 0 & 0 & 0 & 1 \end{bmatrix} \tag{3}$$

where the state transition matrix is defined as $\Phi_{k/k-1}$, and the coefficient $\beta = f_{code}/f_{carrier}$ is used to convert the units of cycles to units of chips [22]. W_k^i denotes the process noise vector of the system. T represents the update period of the navigation filter. Furthermore, the variable $i(i = 1, 2, \cdots, n)$ in the equation denotes a distinct satellite-tracking channel identifier.

The loop filter measurements are output by the loop discriminator, which is represented by the following:

$$Z_k^i = H_k X_k^i + V_k^i \tag{4}$$

$$Z^i = [\Delta\overline{\tau}^i \quad \Delta\overline{\phi}^i]^T \tag{5}$$

$$H_k = \begin{bmatrix} 1 & 0 & \frac{-\beta T}{2} & \frac{\beta T^2}{6} \\ 0 & 1 & -\pi T & \frac{\pi T^2}{3} \end{bmatrix} \tag{6}$$

where the average code phase error and average carrier phase error are defined as $\Delta\overline{\tau}^i$ and $\Delta\overline{\phi}^i$, respectively. V_k^i denotes the observation noise vector.

The early-minus-late phase discriminator was used to determine the code phase error, whereas the two-quadrant arctangent phase discriminator was utilized to determine the carrier error.

$$\Delta\overline{\tau} = \frac{1}{2}(\frac{E-L}{E+L}) \tag{7}$$

$$E = \sqrt{I_E^2 + Q_E^2}, \ L = \sqrt{I_L^2 + Q_L^2} \tag{8}$$

$$\Delta\overline{\phi} = \tan^{-1}(Q_p/I_p) \tag{9}$$

where the coherent integral outputs of the early, later, and prompt forward and quadrature directions of the correlator are represented by I_E, Q_E, I_L, Q_L, I_P, and Q_P.

By adaptively adjusting the measurement noise vector, V_k^i, in low-CNR situations, it is possible to enhance the accuracy of tracking the carrier/code phase. The equation of the measurement noise is as follows [23]:

$$R_k^i = \begin{bmatrix} R_\tau^i & 0 \\ 0 & R_\theta^i \end{bmatrix} \tag{10}$$

$$\begin{cases} R_\tau^i = \sigma_{\Delta\tau^i}^2 t = \frac{d_0 t}{4t CNR^i}(1 + \frac{2}{(2-d_0)t CNR^i}) \\ R_\theta^i = \sigma_{\Delta\theta^i}^2 t = \frac{t}{2t CNR^i}(1 + \frac{1}{2t CNR^i}) \end{cases} \tag{11}$$

where the measurement noise covariance matrix is represented by R_k^i, and A and B indicate the variance of the discriminator outputs. The coherent integration time is denoted as t, and d_0 represents the code spacing between the early and late code replicas [23]. R_τ^i represents the code phase measurement noise, and R_θ^i refers to the carrier phase measurement noise. The CNR for individual channels was calculated by applying the variance sum method to a 20 ms coherent integration output.

Then, the basic equation of the Kalman discrete form for forward filtering is as follows:

$$\begin{cases} \hat{X}_{f,k/k-1}^i = \Phi_{k/k-1}\hat{X}_{f,k-1}^i \\ P_{f,k/k-1}^i = \Phi_{k/k-1}P_{f,k-1}^i\Phi_{k/k-1}^T + Q_k^i \\ K_{f,k}^i = P_{f,k-1}^i H_k^T (H_k P_{f,k/k-1}^i H_k^T + R_k^i) \\ \hat{X}_{f,k}^i = \hat{X}_{f,k-1}^i + K_{f,k}^i(Z_k^i - H_k\hat{X}_{f,k/k-1}^i) \\ P_{f,k}^i = (I_{4\times4} - K_{f,k}^i H_k)P_{f,k/k-1}^i \end{cases} \tag{12}$$

where f indicates the forward filtering process, and the matrix Q_k^i represents the covariance of the system noise.

3.2. RTS Smoothing Algorithm

In the research presented in this paper, the RTS fixed-interval smoothing method was used for filtering the loop structure of vector tracking to improve the model estimation accuracy and reduce the system computational load, thereby achieving a high-precision navigation solution in challenging signal environments. The RTS smoothing algorithm is a commonly used method for processing time-series data that smooths the data by recursively predicting the current state. We adopted a method for reversing the RTS smoothing algorithm from the current time, k, to the $k - 1$ moment to design an RTS filtering model for discrete states. This algorithm effectively eliminated noise and errors in the data, thereby making it more stable and reliable. The data processed using this method can better reflect the real trends and patterns. The design of the RTS algorithm is as follows:

$$\begin{cases} K_{s,k-1}^i = P_{f,k-1}^i \Phi_{k/k-1}^T P_{f,k/k-1}^{-1} \\ \hat{X}_{s,k-1}^i = \hat{X}_{f,k-1}^i + K_{s,k-1}^i (\hat{X}_{s,k}^i - \hat{X}_{s,k/k-1}^i) \\ P_{s,k-1}^i = P_{f,k-1}^i + K_{s,k-1}^i (P_{s,k}^i - P_{f,k/k-1}^i) K_{s,k-1}^T \end{cases} \tag{13}$$

where the subscript s represents the result smoothed by the RTS algorithm, $K_{s,k-1}^i$ represents the filter gain matrix at time $k - 1$, $\hat{X}_{s,k-1}^i$ represents the estimated value of the system state, and $P_{s,k-1}^i$ represents the mean square error matrix of the state estimation.

The loop filter first conducts forward filtering to obtain the intermediate variables for the corresponding Equation (12) in chronological order and then performs the RTS fixed-interval smoothing algorithm in reverse measurement order to complete the entire filtering process of the vector-tracking loop.

4. Navigation Processor for Vector Tracking

4.1. Vector-Tracking Principle

After receiving the GNSS intermediate frequency (IF) signal, each successfully captured satellite was assigned to an independent tracking channel in the vector-tracking loop. The received IF signal was mixed with a locally generated carrier replica. The mixed signal was then correlated with a locally generated code sequence, and the correlator calculated the similarity between the input signal and the local code replica [24]. The correlation results were then integrated and cleared to generate input signals for the carrier loop and code loop discriminators. In the carrier-tracking loop, the phase error of the discriminator is filtered and fed back to a digitally controlled oscillator to adjust the frequency of the local carrier and synchronize it with the transmitted carrier frequency of the satellite. The navigation processor receives this phase error information and converts it into a pseudo-range error and pseudo-range rate error, which are used to estimate the navigation information of the receiver, including position, velocity, and time.

In the research presented in this paper, filtering algorithms and RTS fixed-interval smoothing algorithms were added behind the carrier loop discriminator and code loop discriminator to improve the tracking capability of the vector-tracking loop in weak-signal scenarios and to achieve high-precision navigation in challenging environments.

4.2. Extended Kalman Navigation Filter

The Extended Kalman Filter (EKF) is a state estimation method based on Bayesian theory that effectively handles the state estimation problem of nonlinear systems by combining the system model with observation data. In vector-tracking loops, the EKF algorithm is often used to handle changes in navigation results. Therefore, the system state includes the receiver position errors, ΔP_x, ΔP_y, and ΔP_z; receiver velocity errors, ΔV_x, ΔV_y, and ΔV_z;

receiver clock drift, Δb; and receiver clock drift rate, Δd. The system state equation is defined as follows [25]:

$$\hat{X}_{EKF,k} = \Phi_{EKF,k/k-1}\hat{X}_{EKF,k-1} + \omega_k \tag{14}$$

$$X_{EKF} = \begin{bmatrix} \Delta P_x & \Delta P_y & \Delta P_z & \Delta V_x & \Delta V_y & \Delta V_z & \Delta b & \Delta d \end{bmatrix} \tag{15}$$

$$\Phi_{EKF,k/k-1} = \begin{bmatrix} I_{3\times3} & \tau I_{3\times3} & 0_{3\times2} \\ 0_{3\times3} & I_{3\times3} & 0_{3\times2} \\ 0_{2\times3} & 0_{2\times3} & K \end{bmatrix}, K = \begin{bmatrix} 1 & \tau \\ 0 & 1 \end{bmatrix} \tag{16}$$

where, at time $k-1$ and k, $\hat{X}_{EKF,k-1}$ and $\hat{X}_{EKF,k}$ are used to estimate the system state. Matrix $\Phi_{EKF,k/k-1}$ represents a one-step transition. The data update interval of the navigation processor is denoted as τ. ω_k is the system noise matrix.

The measurement equation of the discrete EKF navigation filter can be expressed as Z_{EKF}:

$$\hat{Z}_{EKF,k} = H_{EKF,k}\hat{X}_{EKF,k} + v_k \tag{17}$$

$$Z_{EKF} = \begin{bmatrix} \Delta\rho^1, \ \Delta\rho^2, \ \cdots \ \Delta\rho^m, \ \Delta\dot{\rho}^1, \ \Delta\dot{\rho}^2, \ \cdots \ \Delta\dot{\rho}^m \end{bmatrix}^T \tag{18}$$

$$H_{EKF,k} = \begin{bmatrix} -\alpha_x^1 & -\alpha_y^1 & -\alpha_z^1 & 0 & 0 & 0 & 1 & 0 \\ -\alpha_x^2 & -\alpha_y^2 & -\alpha_z^2 & 0 & 0 & 0 & 1 & 0 \\ \vdots & \vdots & \vdots & \vdots & \vdots & \vdots & \vdots & \vdots \\ -\alpha_x^m & -\alpha_y^m & -\alpha_z^m & 0 & 0 & 0 & 1 & 0 \\ 0 & 0 & 0 & -\alpha_x^1 & -\alpha_y^1 & -\alpha_z^1 & 0 & 1 \\ 0 & 0 & 0 & -\alpha_x^2 & -\alpha_y^2 & -\alpha_z^2 & 0 & 1 \\ \vdots & \vdots & \vdots & \vdots & \vdots & \vdots & \vdots & \vdots \\ 0 & 0 & 0 & -\alpha_x^m & -\alpha_y^m & -\alpha_z^m & 0 & 1 \end{bmatrix} \tag{19}$$

where $\Delta\rho^i$ and $\Delta\dot{\rho}^i$ denote the inaccuracies in the pseudo-range and range rate measurements for satellite tracking channel $i(i = 1, 2, \ldots, m)$. The variable m denotes the current number of satellites tracked by the GNSS receiver. v_k is the measurement noise vector. $\alpha_x^i, \alpha_y^i, \alpha_z^i (i = 1, 2, \ldots, m)$ represent the line-of-sight distance vectors between the satellites· and the GNSS receiver.

The calculation methods for pseudo-range error, $\Delta\rho^i$, and pseudo-range rate error, $\Delta\dot{\rho}^i$, are as follows:

$$\Delta\rho^i = \Delta\tau^i \cdot \lambda_{code} = \Delta\tau^i \cdot c/f_{code} \tag{20}$$

$$\Delta\dot{\rho}^i = \Delta f^i \cdot \lambda_{carrier} = \Delta f^i \cdot c/f_{carrier} \tag{21}$$

where λ_{code} and $\lambda_{carrier}$ are the wavelengths of the C/A code and the carrier, respectively; and c represents the speed of light.

5. Experiment and Analysis

The performance of the vector-tracking loop proposed in the research presented in this paper was validated through motion experiments conducted on shipborne equipment. The equipment used in the experiment is shown in Figure 2. An electric rubber boat was used as the motion carrier of the experiment, and a laptop was installed on it to store all data collected in the experiment. An IF signal collector was used to collect the IF signals from the navigation satellites. A Trimble BD992 high-precision navigation receiver was used to obtain the navigation parameters of the carrier for reference and comparison. Two antennas were used to obtain the signals of the IF collector and navigation receiver. The performances of the GNSS navigation receiver and IF signal collector are shown in Tables 1 and 2.
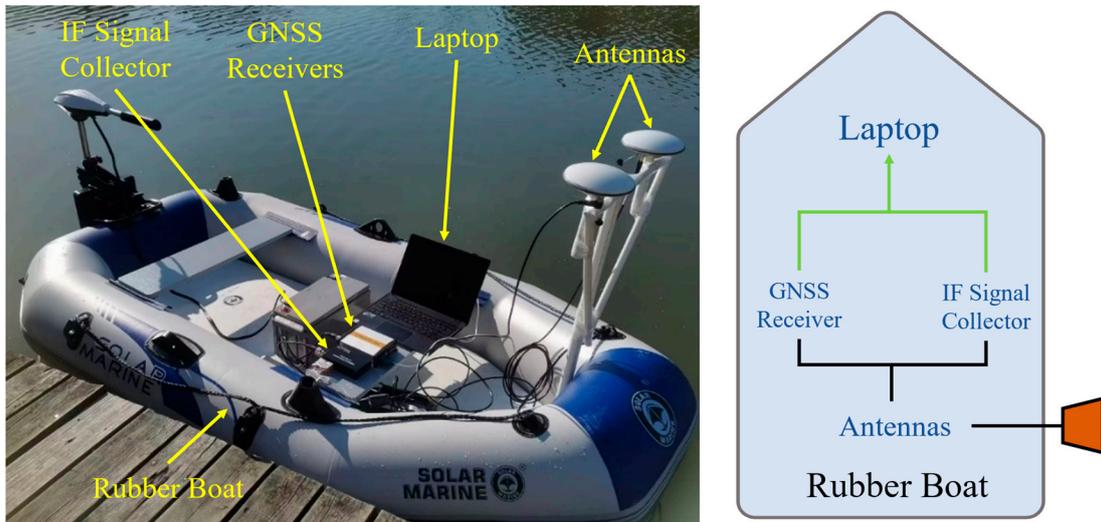
Figure 2. Experimental equipment.

Table 1. The performance of the Trimble BD992 receiver.

Equipment Model	Horizontal Position Accuracy	Horizontal Velocity Accuracy
Trimble BD992	0.5 m	0.007 m/s

Table 2. The performance of the IF signal collector.

Equipment Model	GNSS Frequency	GPS IF	Sampling Frequency
HG—SOFTGPS02	GPS L1 C/A	3.996 MHz	16.369 MHz

In this experiment, we chose a river with an occluded environment as the experimental path, with a length of approximately 600 m. The blue line in Figure 3 represents the experimental trajectory. The river has a complex environment, providing excellent natural conditions for simulating application scenarios when satellite signals are occluded. To simulate the actual environment more realistically, we used two single bridges and a double bridge across the middle of the river as signal blockers to test signal tracking under different occlusion conditions.

Figure 3. Experimental path.

The bridge width of signal-blocking area 1 is approximately 14 m, as shown in Figure 4a. The bridge width of signal-blocking area 2 is approximately 21 m, as shown in

Figure 4b. Signal-blocking area 3 consists of two bridges separated by a distance of 6 m, with each bridge having a width of roughly 25 m, resulting in a total signal blockage area across an expanse of approximately 56 m, as shown in Figure 4c.

(**a**) Signal-blocking area 1.

(**b**) Signal-blocking area 2.

(**c**) Signal-blocking area 3.
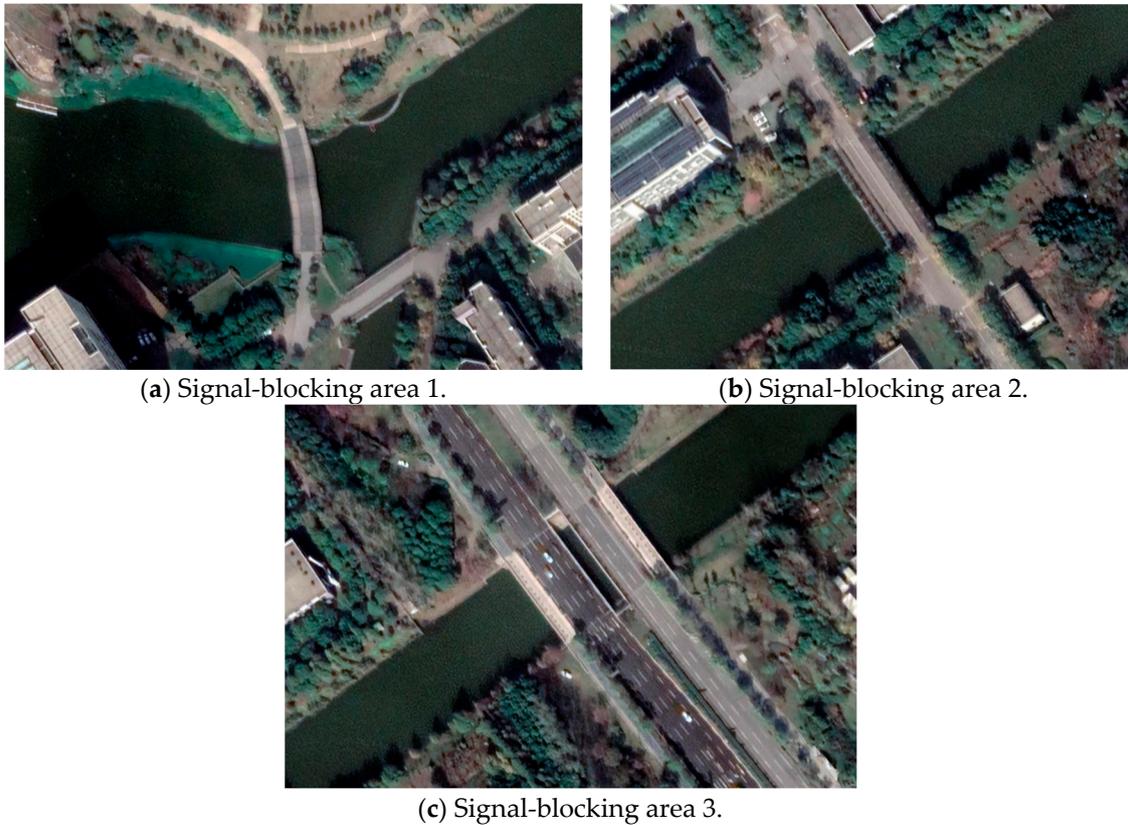
Figure 4. Signal-blocking environment.

During the experiment, the initial position remained stationary for at least 30 s to ensure the accurate acquisition and tracking of the loop. Subsequently, following a brief acceleration period of approximately 5 s, the experimental setup was maintained at a constant speed until it reached the final position. The duration of the experiment was approximately 400 s.

5.1. The Analysis of Signal-Tracking Loops

The tracking performance of the receiver on GNSS signals directly affects the accuracy of positioning results. Therefore, to analyze the signal-tracking performance of the vector-tracking loop based on the RTS smoothing algorithm proposed in this paper, the signal-tracking situation of the proposed method is compared with the traditional STL, traditional VTL, and Kalman Filter-based VTL.

In this experiment, seven visible satellites were successfully captured and tracked, as shown in Figure 5. During the experiment, we set the elevation mask angle to 15° and recorded the positions of the satellites in the sky, as shown in Figure 6.

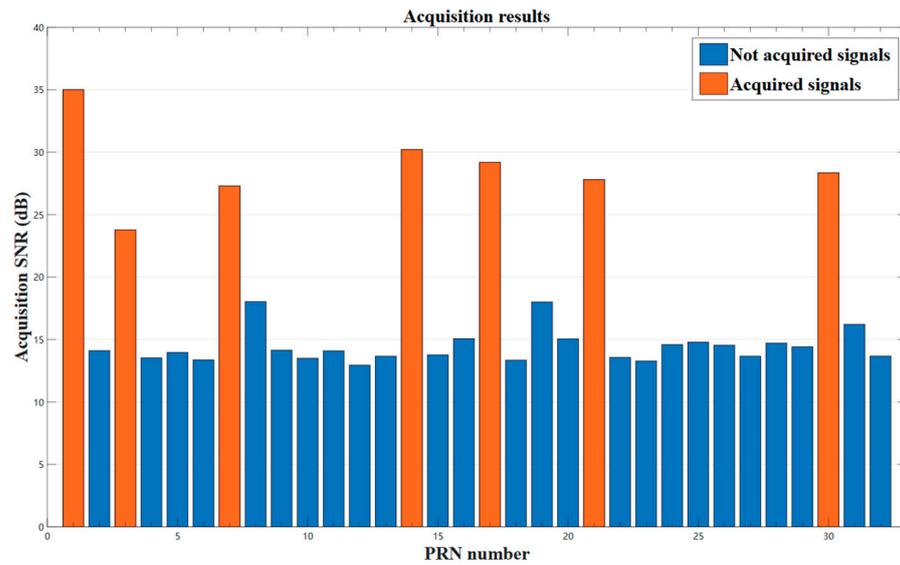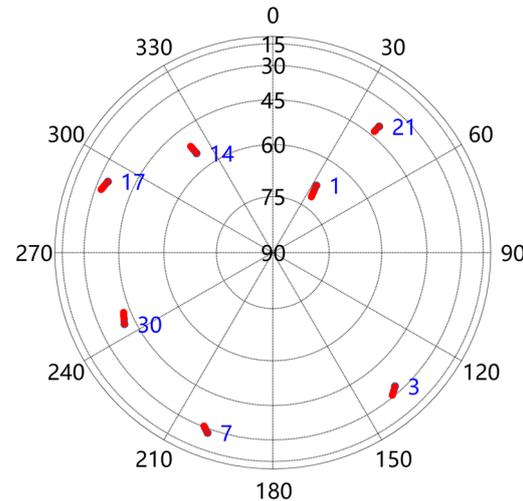**Figure 5.** Satellites acquisition result.

Figure 6. Sky map of the satellite tracked during the experiment. (The number indicates the corresponding satellite PRN number).

The carrier-to-noise ratio of the satellite signal during the entire experiment is shown in Figure 7a. It can be observed that, during the periods from 106 s to 118 s, 232 s to 250 s, and 322 s to 362 s, the value of the carrier-to-noise ratio of the satellite signal rapidly decreased from 35 dB-Hz to below 30 dB−Hz, indicating that the rubber boat was located beneath corresponding obstructions, such as bridges. This indicates that the received satellite signal was severely obstructed during these time periods, and it can be inferred from the figure that the duration of the signal obstruction is proportional to the length of the bridge. The carrier-to-noise ratio image of the signal-blocking area is shown in Figure 7b–d.
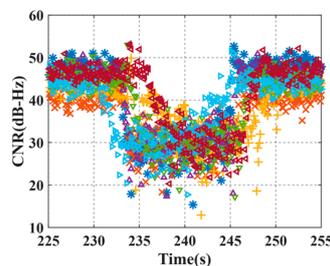
This paper compares the tracking loops of visible satellites, PRN3 and PRN14, in the experimental process and conducts a comparative analysis of their tracking carrier frequency and code phase, as shown in Figures 8 and 9.
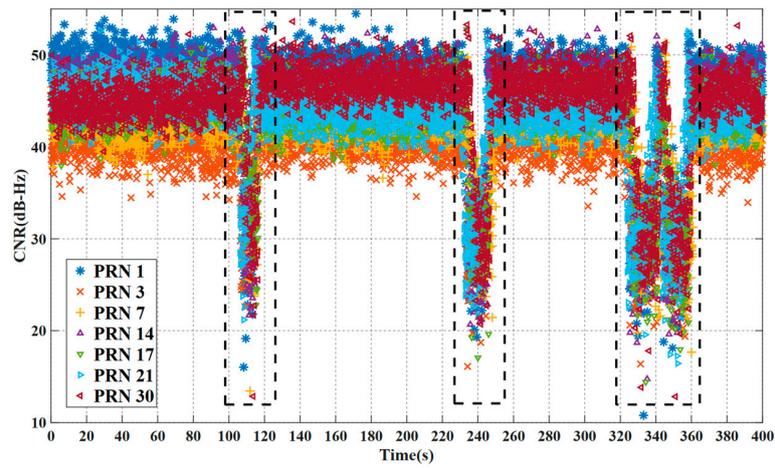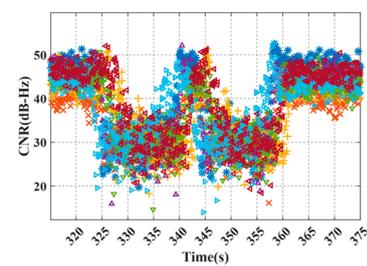
(**a**) The carrier-to-noise ratio during the whole experiment.
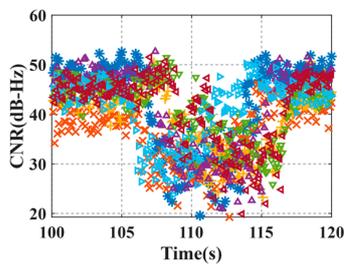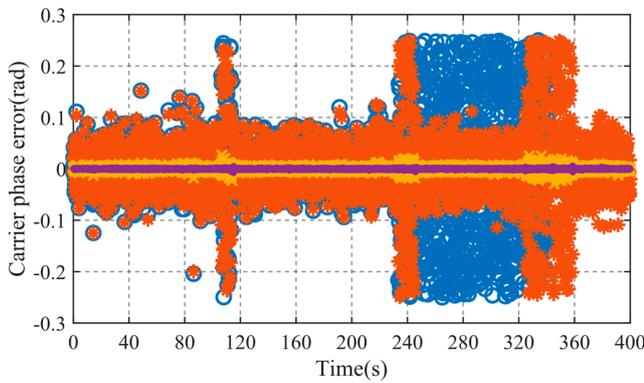

(**b**) Signal-blocking area 1.
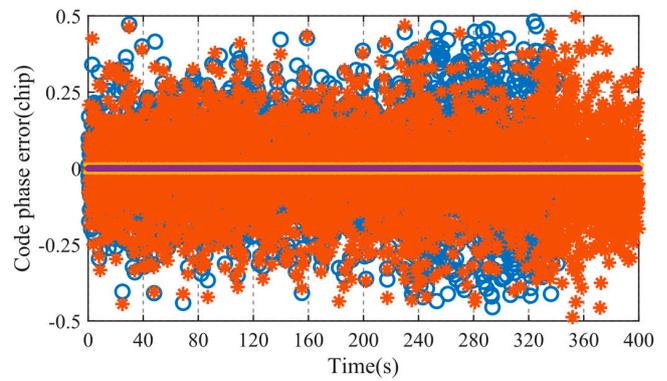
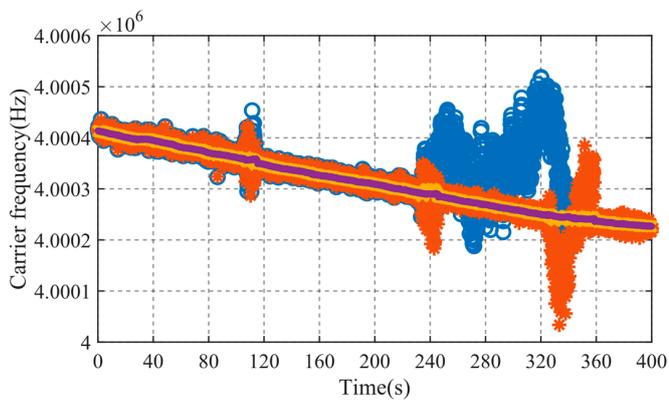(**c**) Signal-blocking area 2.

(**d**) Signal-blocking area 3.

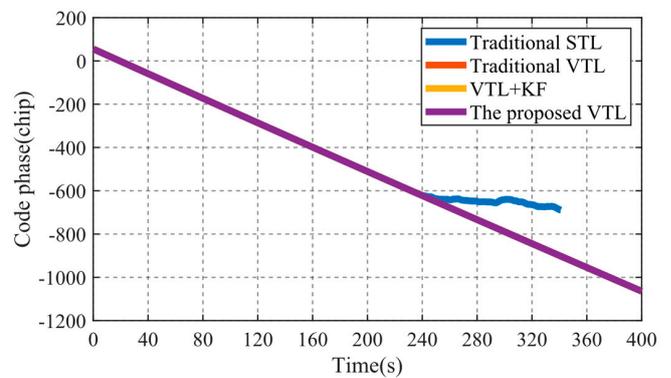**Figure 7.** Carrier-to-noise ratio.

(**a**) Carrier phase error of PRN 3.

(**b**) Code phase error of PRN 3.

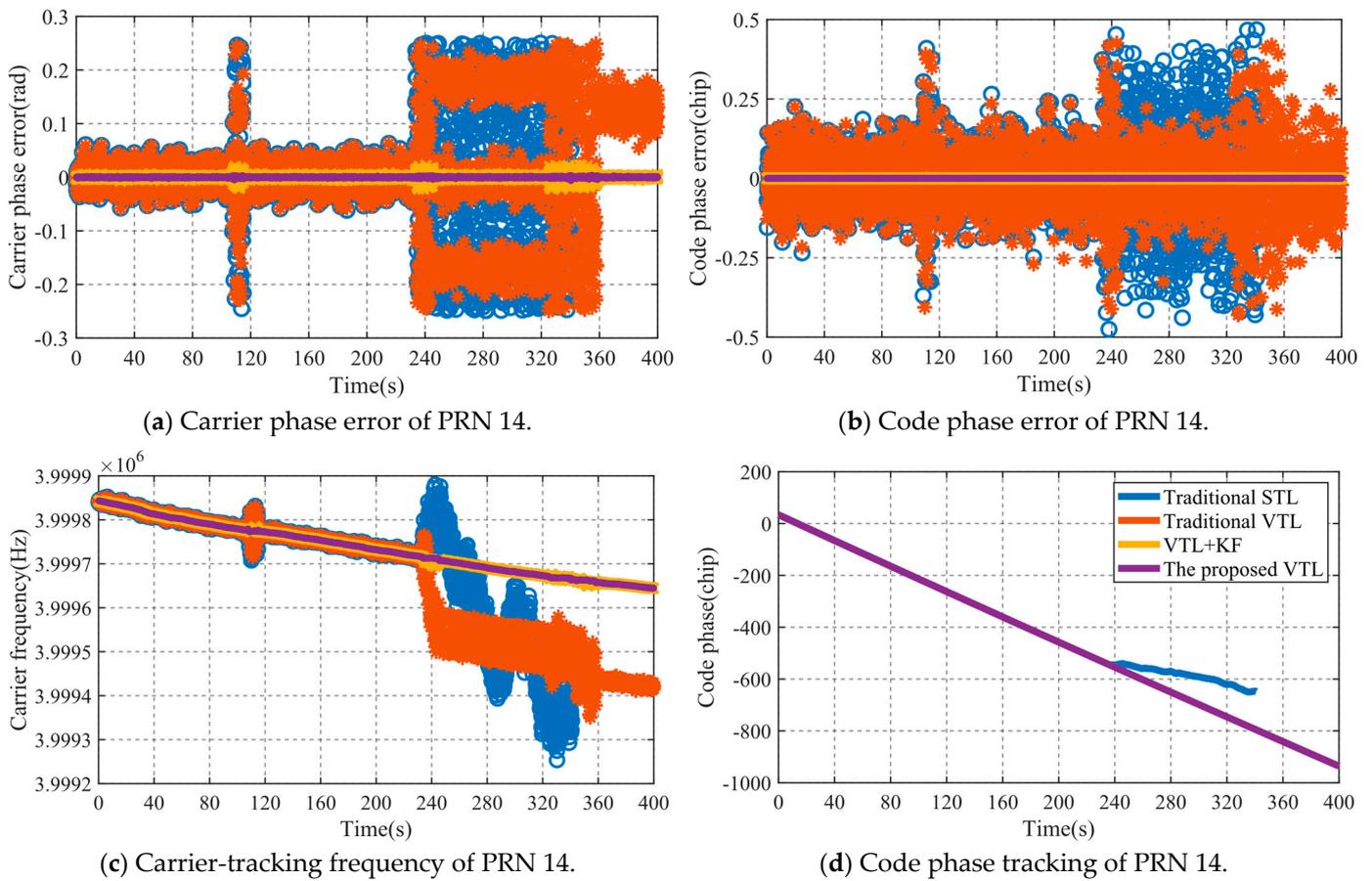(**c**) Carrier-tracking frequency of PRN 3.

(**d**) Code phase tracking of PRN 3.

Figure 8. Information on the tracking loop of PRN 3.

(**a**) Carrier phase error of PRN 14.

(**b**) Code phase error of PRN 14.

(**c**) Carrier-tracking frequency of PRN 14.


(**d**) Code phase tracking of PRN 14.

Figure 9. Information on the tracking loop of PRN 14.

As shown in Figure 8a,c, the tracking of the carrier by the loop is relatively stable in an open-sky environment, with fluctuations within a range of 0.2 radians. When the rubber boat reached the first signal obstruction at 106 s, the carrier phase error of the traditional method quickly increased to 0.5 radians and then returned to normal when the rubber boat left the obstructed area at 118 s. However, during the experiment at 250 s, when the rubber boat left the second obstructed area, it can be seen that traditional STL (indicated in blue) locked onto an incorrect carrier frequency after signal interruption and maintained a high level of error. The traditional VTL (indicated in orange), benefiting from coupling between signal channels, was able to quickly recover the tracking of signals after leaving obstructions. After passing through the third obstructed environment, where the obstruction time was longer, the traditional STL could no longer continue tracking signals, as its loop was interrupted and needed to reacquire satellite signals. Figure 8b,d show the code phase and code phase error of PRN 3. Adding loop filtering can effectively reduce the code phase error of the loop and improve navigation accuracy in signal-obstructed environments. Compared to the other three methods, the proposed method makes loop tracking more stable and achieves better accuracy in carrier and code tracking.

The carrier- and code-tracking processes of the PRN14 satellite exhibit lower carrier and code phase errors than PRN3 in unobstructed environments. As shown in Figure 9a,c, from the 232 s, when the bridge begins to obstruct the signal path, the traditional STL phase error gradually increases, eventually leading to a loop loss of lock. Meanwhile, traditional VTL locks onto the wrong carrier frequency after 250 s, resulting in large carrier phase errors that directly affect the navigation accuracy. Compared with the other three schemes, the proposed loop structure can maintain the accuracy of both carrier phase and code phase measurements, providing higher precision measurement values for navigation filters, not only improving navigation accuracy but also enhancing loop performance.

5.2. The Analysis of Navigation Results

The results of the navigation experiment are shown on the map in Figure 10a. The specific location results of the occluded areas are shown in Figure 10b–d. The experiment used the positioning results of the Trimble BD992 receiver as the reference motion trajectory for the rubber boat and compared the traditional STL, traditional VTL, KF-filtered VTL, and RTS smoothing algorithm-based VTL proposed in this paper. As can be seen from the disconnected green line in Figure 10d, the Trimble BD992 receiver may fail to output navigation results when encountering long-term satellite-signal blockages. Therefore, to compare the real experimental route, the rubber boat was kept at a constant speed and straight-line motion during the experiment. The position of the blocked area is calculated by interpolating between reliable position points on both sides of the obstruction and ultimately fitting a credible reference path. The fitted reference path is shown by black lines, A-B, in Figure 11. The velocity results for the entire experiment are shown in Figure 12. The following section analyzes the navigation performance of the four loop tracking schemes in different occlusion environments.
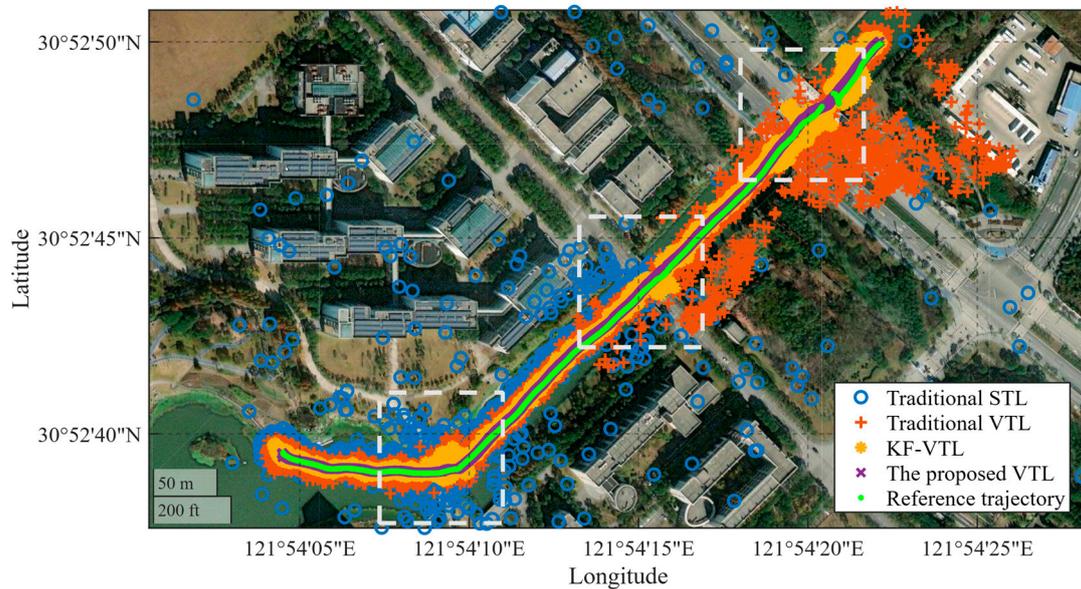
(**a**) The whole position results of the experiment.
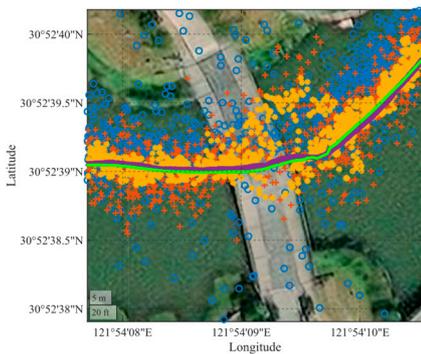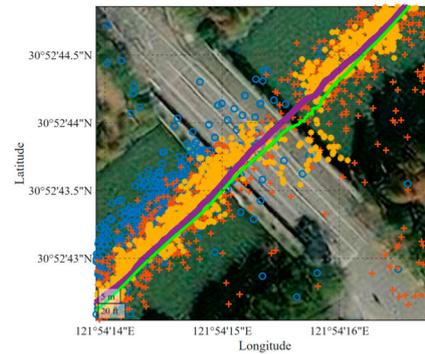
(**b**) Signal-blocking area 1.　　　　(**c**) Signal-blocking area 2.　　　　(**d**) Signal-blocking area 3.

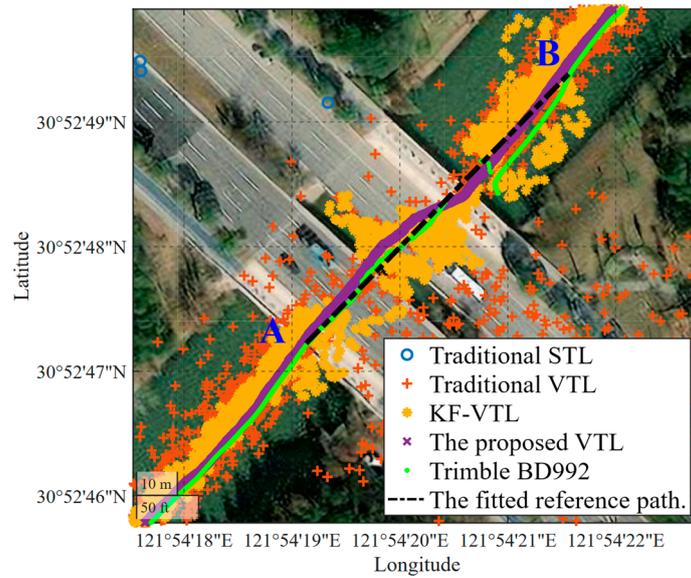**Figure 10.** Comparison of navigation results of different methods.

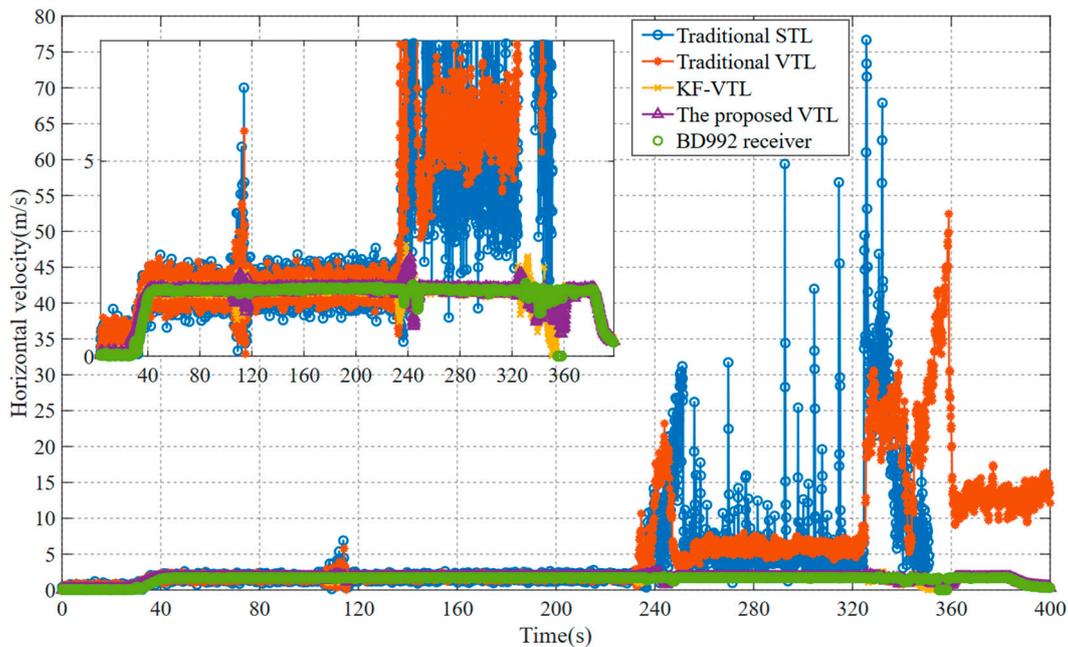**Figure 11.** The reference path of signal-blocking area 3.

Figure 12. The velocity results of the experiment.

Figure 10b shows when the rubber boat reaches the first bridge. Figure 13 shows the horizontal position and horizontal velocity errors during this process. It can be observed from Table 3 that, in a signal-obstructed environment, the traditional STL exhibits a larger horizontal position error and horizontal velocity error than the other three methods. Compared with the STL, the traditional VTL demonstrated a superior signal-tracking performance in weak-signal environments, reducing the horizontal position error by 68.1% and the horizontal velocity error by 23.9%. This observation aligns with the theoretical description of the vector-tracking performance. The introduction of a KF can improve the signal-tracking accuracy of the VTL loop. The comparison between traditional VTL and KF-VTL methods reveals a significant improvement in the RMSE of horizontal position, from 15.54 m to 7.61 m, representing an increase in accuracy of 51.1%. Additionally, there is a notable enhancement in the RMSE of horizontal velocity, which decreases from 0.83 m/s to 0.24 m/s, resulting in an increase in accuracy of 70.4%. Furthermore, the proposed

method adds a backward RTS smoothing process to the forward KF, thereby demonstrating better navigation accuracy, which achieved an RMSE of 0.95 m for horizontal position and an RMSE of 0.24 m/s for horizontal velocity at blocking area 1, improving accuracy by 93.9% and 71.1% compared to traditional VTL. The specific error parameters are listed in Table 3.
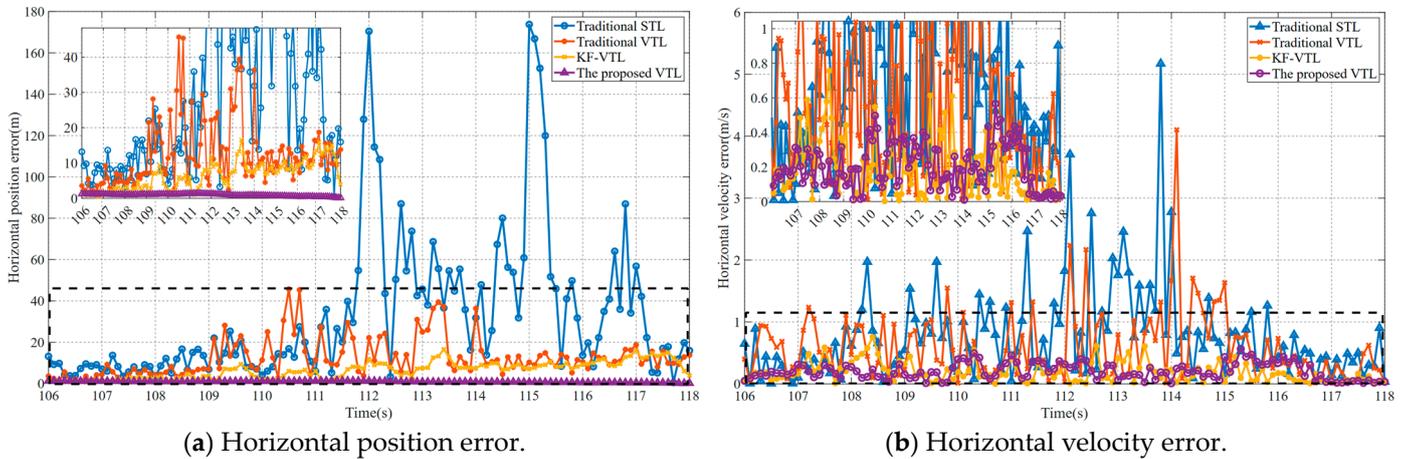

(**a**) Horizontal position error. (**b**) Horizontal velocity error.

Figure 13. Error of navigation results in signal-blocking area 1.

Table 3. Horizontal position error and horizontal velocity error in signal-blocking area 1.

Method	Horizontal Position (m)		Horizontal Velocity (m/s)	
	RMSE	Max	RMSE	Max
Traditional STL	48.73	173.79	1.09	5.17
Traditional VTL	15.54	45.66	0.83	4.10
KF—VTL	7.61	16.53	0.25	0.76
The proposed VTL	0.95	1.34	0.24	0.56

Figure 14 shows the horizontal position error and horizontal velocity error of the four methods during the period 222 s–260 s. From 232 s to 250 s, the rubber boat moved under the second bridge. The position RMSE and velocity RMSE of the four methods in the occlusion environment from 232 s to 250 s are summarized in Table 4. The interruption of satellite signals resulted in the traditional STL losing its lock, leading to a significant increase in the horizontal position and velocity errors. The maximum horizontal position error reached 6006.24 m, and the maximum horizontal velocity error reached 29.46 m/s, which is far beyond the acceptable range. The traditional VTL also showed significant deviations in the measurement of position and velocity during signal occlusion, reaching 41.6 m and 9.86 m/s, respectively. Compared with the traditional VTL method, the VTL method based on KF filtering significantly improves accuracy. The horizontal position error decreased from 41.6 m to 8.55 m, an increase in accuracy of 79.4%, and the horizontal velocity error decreased from 9.86 m/s to 0.45 m/s, an increase in accuracy of 95.4%. Compared with the traditional VTL method, the proposed method can reduce the horizontal position error from 41.6 m to 1.75 m, with an accuracy improvement of 95.8%. The horizontal velocity error is reduced from 9.86 m/s to 0.41 m/s, with an accuracy improvement of 95.8%. By comparison, it is found that the STL method loses lock after a signal obstruction of 18 s, leading to the rapid divergence of navigation errors and system unavailability, while the three VTL methods do not lose lock during this process, demonstrating excellent dynamic performance under weak signals. The method proposed in this paper achieved the highest accuracy and stability among the four methods.
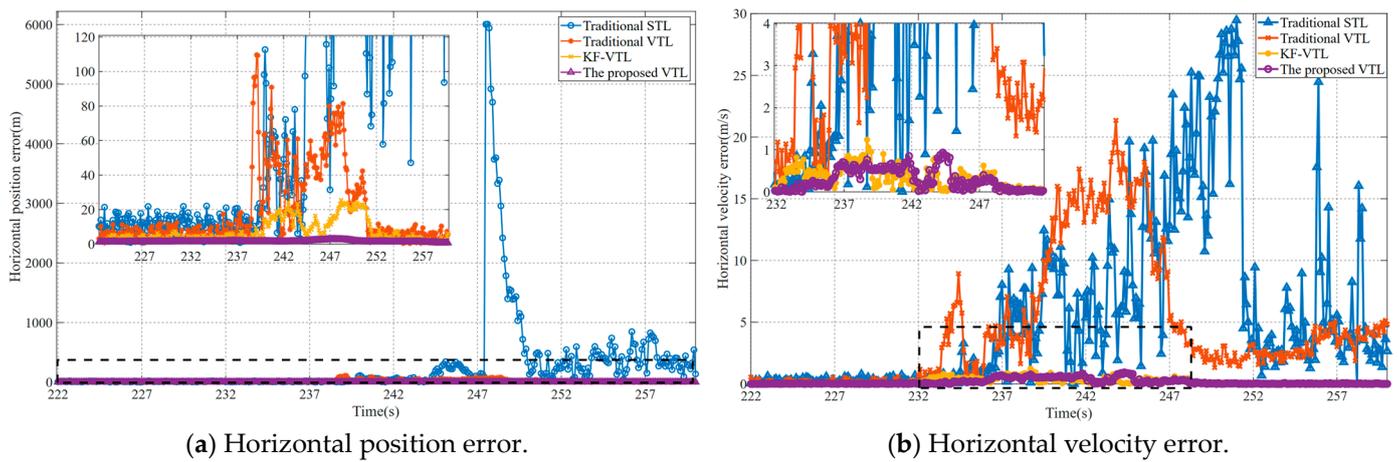
(**a**) Horizontal position error.

(**b**) Horizontal velocity error.

Figure 14. Error of navigation results in signal-blocking area 2.

Table 4. Horizontal position error and horizontal velocity error in signal-blocking area 2.

Method	Horizontal Position (m)		Horizontal Velocity (m/s)	
	RMSE	Max	RMSE	Max
Traditional STL	1164.28	6006.24	10.21	29.46
Traditional VTL	41.60	109.63	9.86	21.35
KF—VTL	8.55	25.50	0.45	1.24
The proposed VTL	1.75	2.68	0.41	0.93

Although introducing the KF into the VTL can effectively improve the satellite signal-tracking capability and navigation performance of the navigation system in weak-signal environments, comparative experimental results show that there is still a significant navigation position error in obstructed environments. As shown in Figure 14 and Table 4, the maximum horizontal position error of KF-VTL is 25.50 m, with an RMSE of 8.55 m; and the proposed method reduces the maximum horizontal position error to 2.68 m, with an RMSE of 1.75, so the accuracy is significantly improved.

The position and velocity errors of the rubber boat passing through the third signal-blocking area during the experiment are shown in Figure 15. The signal obstructions are two bridges with a total length of 56 m, as shown in Figure 11. Because of the obstruction above the experimental rubber boat, the signal was blocked for approximately 40 s. The traditional VTL has large position and velocity errors during the signal obstruction process; however, it can quickly capture the corresponding signals at the midpoint between the two bridges to reduce errors. The traditional VTL position RMSE is 62.63 m, and the velocity RMSE is 23.82 m/s during passing through these two bridges. Although VTL based on the KF can maintain stable tracking of signals in obstructed environments, its output errors continue to fluctuate, and its accuracy is not high, with a position RMSE of 9.65 m and a velocity RMSE of 0.59 m/s. The VTL based on KF-RTS smoothing is capable of maintaining stable signal tracking even during prolonged signal obstructions, while also achieving high accuracy in position and velocity estimation, with a position RMSE of 3.47 m and a velocity RMSE of 0.57 m/s, thus demonstrating an excellent navigation performance. Compared with the traditional VTL method, the proposed method reduced the horizontal position error by 94.5% and horizontal velocity error by 97.6%. The comprehensive results of the position RMSE and velocity RMSE in the third signal-blocking area for the three methods are summarized in Table 5.
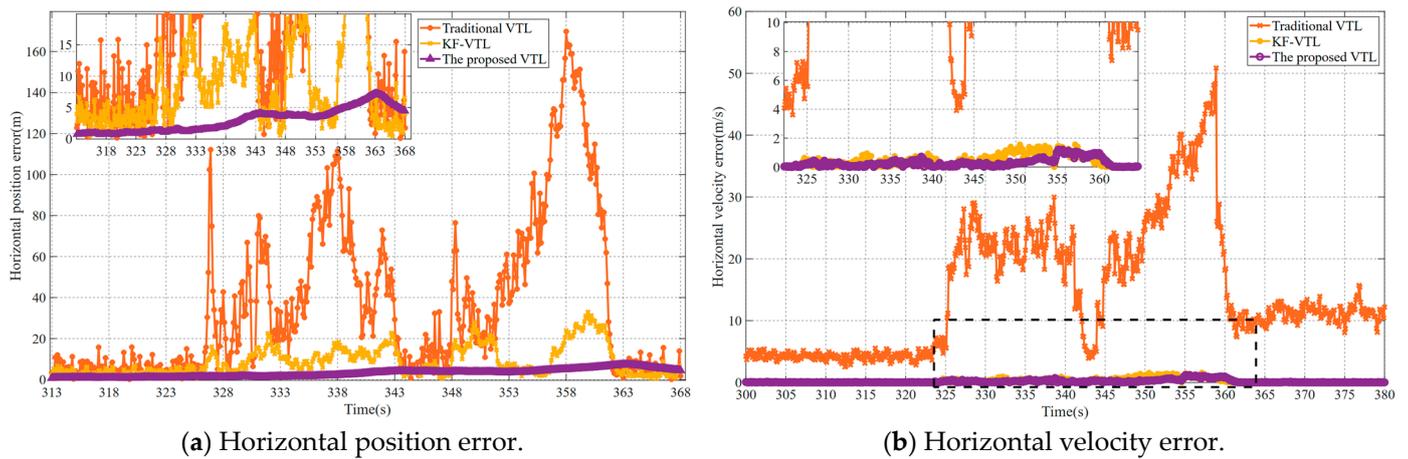
(**a**) Horizontal position error.

(**b**) Horizontal velocity error.

Figure 15. Error of navigation results in signal-blocking area 3.

Table 5. Horizontal position error and horizontal velocity error in signal-blocking area 3.

Method	Horizontal Position (m)		Horizontal Velocity (m/s)	
	RMSE	Max	RMSE	Max
Traditional VTL	62.63	169.74	23.82	50.84
KF—VTL	9.65	32.94	0.59	1.56
The proposed VTL	3.47	7.26	0.57	1.21

6. Conclusions

This paper presents a VTL framework utilizing the forward KF and backward RTS smoothing algorithm, aiming to enhance the signal-tracking capability of navigation receivers in occluded environments, improve the stability of navigation systems, and increase robustness in weak-signal scenarios. This article provides a detailed introduction to the composition and structure of the VTL, the algorithmic structure of loop filters, and the basic principles of navigation filters based on the EKF. As an important component of VTL, loop filters are mainly used to filter the output of tracking loops to reduce noise and improve tracking accuracy. The research work focuses on designing a bidirectional loop filter based on forward KF and backward RTS and verifies its performance through experiments. Compared with traditional STL, traditional VTL, and KF-based VTL methods, the new method shows a superior performance, with significant effects on enhancing the signal-tracking capability of receivers in weak-signal environments, while ensuring positioning accuracy and robustness of navigation systems.

Author Contributions: Conceptualization, Y.H. and W.L.; methodology, N.L. and L.W.; software, L.W.; validation, L.W., W.L. and N.L.; resources, N.L.; data curation, L.W.; writing—original draft preparation, L.W.; writing—review and editing, W.L.; visualization, L.W.; supervision, Y.H.; project administration, W.L.; funding acquisition, W.L. All authors have read and agreed to the published version of the manuscript.

Conflicts of Interest: The authors declare no conflicts of interest.

References

1. Lashley, M.; Bevly, D.M.; Hung, J.Y. Performance Analysis of Vector Tracking Algorithms for Weak GPS Signals in High Dynamics. *IEEE J. Sel. Top. Signal Process.* **2009**, *3*, 661–673. [CrossRef]
2. Han, Z.; Liu, D.; Wei, Z.; Xu, Y.; Li, R. A Carrier phase tracking method for vector tracking loops. *Gps Solut.* **2022**, *26*, 111. [CrossRef]

3. Jee, G.-I.; Im, S. Performance Evaluation of Vector Tracking Loop Based Receiver for GPS Anti-Jamming Environment. *J. Inst. Control Robot. Syst.* **2013**, *19*, 152–157. [CrossRef]
4. An, Q.; Li, C.; An, H. Review on vector tracking application to GNSS receiver. In Proceedings of the 12th IEEE International Conference on Electronic Measurement and Instruments (ICEMI), Qingdao, China, 16–18 July 2015; pp. 318–323.
5. Hsu, L.-T.; Jan, S.-S.; Groves, P.D.; Kubo, N. Multipath mitigation and NLOS detection using vector tracking in urban environments. *Gps Solut.* **2015**, *19*, 249–262. [CrossRef]
6. Kim, K.-H.; Jee, G.-I.; Im, S.-H. Adaptive Vector-tracking Loop for Low-quality GPS Signals. *Int. J. Control Autom. Syst.* **2011**, *9*, 709–715. [CrossRef]
7. Lin, H.; Huang, Y.; Tang, X.; Sun, G.; Ou, G. A robust vector tracking loop based on diagonal weighting matrix for navigation signal. *Adv. Space Res.* **2017**, *60*, 2607–2619. [CrossRef]
8. Park, M.; Kee, C. Frequency Tracking Error Analysis of LQG Based Vector Tracking Loop for Robust Signal Tracking. *J. Position. Navig. Timing* **2020**, *9*, 207–214. [CrossRef]
9. Liu, W.; Huang, H.; Hu, Y.; Mou, M.; Hsieh, T.-H.; Hu, Q.; Wang, S. Improved GNSS vector tracking loop to enhance the navigation performance of USV. *Ocean Eng.* **2022**, *258*, 111865. [CrossRef]
10. Xia, J.; Yue, F.Z.; Wang, P.P.; Wang, S. Robust gnss signal tracking algorithm based on vector tracking loop under ionospheric scintillation conditions. In Proceedings of the 12th IEEE International Conference on Signal Processing (ICSP), Hangzhou, China, 19–23 October 2014; pp. 2385–2389.
11. Won, J.-H.; Eissfeller, B.; Pany, T. Implementation, Test and Validation of a Vector-Tracking-Loop with the ipex Software Receiver. In Proceedings of the 24th International Technical Meeting of the Satellite Division of the Institute of Navigation (ION GNSS), Portland, OR, USA, 20–23 September 2010; pp. 795–802.
12. Dai, X.; Nie, J.; Chen, F.; Ou, G. Distortionless space-time adaptive processor based on MVDR beamformer for GNSS receiver. *Iet Radar Sonar Navig.* **2017**, *11*, 1488–1494. [CrossRef]
13. Jakubov, O.; Kovar, P.; Kacmarik, P.; Vejrazka, F. Distributed Extended Kalman Filter for Position, Velocity, Time Estimation in Satellite Navigation Receivers. *Radioengineering* **2013**, *22*, 776–790.
14. Yan, Z.; Ruotsalainen, L.; Chen, X.; Tang, X. An INS-assisted vector tracking receiver with multipath error estimation for dense urban canyons. *Gps Solut.* **2023**, *27*, 88. [CrossRef]
15. Gan, X.; Li, W.; Yang, L.; Zhang, H. State-Space Measurement Update for GNSS/INS Integrated Navigation. *Math. Probl. Eng.* **2020**, *2020*, 3675824. [CrossRef]
16. Liu, S.; Li, S.; Fu, Q.; Tao, Y.; Wu, F. A New MIMU/GNSS Ultra-Tightly Coupled Integration Architecture for Mitigating Abrupt Changes of Frequency Tracking Errors. *Micromachines* **2020**, *11*, 1117. [CrossRef] [PubMed]
17. Qin, F.; Zhan, X.; Zhan, L. Performance assessment of a low-cost inertial measurement unit based ultra-tight global navigation satellite system/inertial navigation system integration for high dynamic applications. *Iet Radar Sonar Navig.* **2014**, *8*, 828–836. [CrossRef]
18. Zhu, Z.; Jiang, C.; Bo, Y. Performance Enhancement of GNSS/MEMS-IMU Tightly Integration Navigation System Using Multiple Receivers. *IEEE Access* **2020**, *8*, 52941–52949. [CrossRef]
19. Zhang, Q.; Niu, X.; Zhang, H.; Shi, C. Algorithm Improvement of the Low-End GNSS/INS Systems for Land Vehicles Navigation. *Math. Probl. Eng.* **2013**, *2013*, 435286. [CrossRef]
20. Abdel-Hafez, M.F. The Autocovariance Least-Squares Technique for GPS Measurement Noise Estimation. *IEEE Trans. Veh. Technol.* **2010**, *59*, 574–588. [CrossRef]
21. Tang, X.; Falco, G.; Falletti, E.; Lo Presti, L. Complexity reduction of the Kalman filter-based tracking loops in GNSS receivers. *Gps Solut.* **2017**, *21*, 685–699. [CrossRef]
22. Tang, X.; Yang, Y.; Chen, X.; Falco, G.; Falletti, E. A Newly Designed Tracking Loop for Power-saving Receivers. In Proceedings of the 4th IEEE International Conference on Ubiquitous Positioning, Indoor Navigation and Location Based Services (IEEE UPINLBS), Shanghai, China, 2–4 November 2016; pp. 102–106.
23. Liu, W.; Huang, H.; Hu, Y.; Han, B.; Wang, S.Z. A robust GNSS sensors in presence of signal blockage for USV application. *Meas. Sci. Technol.* **2024**, *35*, 035124. [CrossRef]
24. Harima, K.; Saito, H.; Ebinuma, T. Navigation message demodulation for GPS receiver on-board spinning rockets. *Gps Solut.* **2012**, *16*, 495–505. [CrossRef]
25. Yang, H.; Zhou, B.; Wang, L.; Wei, Q.; Ji, F.; Zhang, R. Performance and Evaluation of GNSS Receiver Vector Tracking Loop Based on Adaptive Cascade Filter. *Remote Sens.* **2021**, *13*, 1477. [CrossRef]